GI_Forum 2023, Issue 2
Page: 32 - 46
Full Paper
Corresponding Author:
natalia.kolecka@wsl.ch
DOI: 10.1553/giscience2023_02_s32

# Airborne LiDAR Enables Measurements of "Greenness" Observed from the Human Perspective

Natalia Kolecka[1], Christian Ginzler[1], Maria Garcia Martin[1] and Silvia Tobias[1]

[1]Swiss Federal Institute for Forest, Snow and Landscape Research WSL, Birmensdorf, Switzerland

**Abstract**

Green spaces and natural environments are essential for quality of life, as they influence health behaviours and outcomes positively. The quantification of "greenness" observable from the human perspective is of great interest, especially in urban environments where built-up areas and infill are expanding. In this paper, we present a method based on airborne laser scanning (ALS) point clouds that makes it possible to simulate a space observed from the human perspective and to quantify the surrounding vegetation. The method can be applied over various spatial scales, in urban, suburban and rural regions. We employed this new method to analyse a set of specific locations in Switzerland that are important for people to recover from everyday stress. The greenness quantification can be used to compare the perceived restorative quality of landscape characteristics with physical landscape qualities. Our approach provides a viable methodological solution for spatial planning and large-scale socio-ecological studies on the influence of natural and green spaces on health and wellbeing, and we recommend that it be applied in the natural landscape and in urban areas.

**Keywords:**

GIS, green space, LiDAR, restoration, vegetation

## 1 Introduction

Urban areas worldwide are experiencing continuous population growth (World Bank, 2022) and, consequently, continuous expansion of their extent and infill development. Green spaces and natural environments are essential for urban quality of life (Bell, 2010) as they affect health behaviours and outcomes positively (Bezold et al., 2018; James, Banay, Hart, & Laden, 2015; Wood, Hooper, Foster, & Bull, 2017). Switzerland has a predominantly urban population, with 74% of inhabitants living in cities and conurbations in 2022 (World Bank, 2022). Thus, the quality of, and accessibility to, green and natural spaces in and near urban areas are of great interest in this country. Access to green spaces and vegetation, or its visibility, has a major impact on people's wellbeing (Palliwoda & Priess, 2021). This is currently being investigated

in the interdisciplinary research project RESTORE (https://www.wsl.ch/de/projekte/noise-and-greenspaces.html).

Objective (quantitative) two- and three-dimensional measures of the biomass and canopy cover as well as of the structure and spatial patterns of vegetation can be obtained from spatial data. However, the quantification of "greenness" from the human perspective (i.e. how much vegetation is actually visible) using spatial data is not trivial and, to the best of our knowledge, studies on this topic (e.g., Kumakoshi, Chan, Koizumi, Li, & Yoshimura, 2020; Labib, Huck, & Lindley, 2021; Li et al., 2015; Yu et al., 2016) have not provided a widely accepted solution. Much research has involved measuring greenness using remote sensing data (e.g., Degerickx, Hermy & Somers, 2020; review by Shahtahmassebi et al., 2021). Satellite-based vegetation indices, such as the Normalized Difference Vegetation Index (NDVI), the Green-Red Vegetation Index (GRVI) and the Enhanced Vegetation Index (EVI), are widely used and represent the density and health of vegetation (Zeng et al., 2022). They are also used to map land use/land cover and can be used to calculate the percentage of a spatial area covered by various types of green space (e.g., parks, public gardens, sports fields, forests). These 2D data may provide information on general features of a certain area, but they give a simplified representation of vegetation and may miss details, such as "green" or "living" walls, or lawns and shrubs under tree canopies, which are crucial elements in a human's field of view (Li et al., 2015; Yang, Zhao, Mcbride, & Gong, 2009).

Many of these limitations can be overcome by airborne laser scanning (ALS) data, which are widely used in the domain of forestry. ALS data make it possible to describe the horizontal and vertical vegetation structure in 3D, to count single trees and measure their parameters (e.g., crown radius and height, trunk height), and even to perform crown-shape-based recognition of tree species (Goodbody et al., 2020; Pirotti, 2011). Descriptions of vegetation based on ALS point clouds incorporate metrics related to a spatial unit (pixel, voxel, surroundings of a particular location) or to a single tree (Roussel et al., 2020).

Quantifying greenness from the human perspective (i.e. the amount of vegetation observable in one's surroundings) involves either analysis of photographs taken from a fixed location, or geospatial modelling. The first approach involves the calculation of the proportion of vegetation pixels in photographs and panoramic images taken from street level (Yang et al., 2009). Some research has aided photography-based analysis by relating it to spatial data, in particular ALS (Chen, Xu, & Gao, 2015) or satellite imagery from Google Earth (Jiang et al., 2017). Even though the authors of these studies emphasized the good performance of their methods, the photography-based approach has several weaknesses. 2D images do not provide information about the distance to the vegetation or its density, which are important aspects of the visual significance of observed objects (Aben, Pellikka & Travis, 2018; Nutsford, Reitsma, Pearson & Kingham, 2015). Additionally, 2D images exaggerate the proportion of greenness towards the zenith (at larger vertical angles). Moreover, even when street-view imagery databases are included (e.g., Google or Baidu), the methods are spatially limited by the availability of photos (usually to streetscapes with vehicular access) and thus are not suitable for analysing large regions. The greatest drawback is that identifying vegetation in street-level

photographs and satellite imagery can be labour-intensive, as it has to be carried out manually using an image editing software.

The second approach, geospatial modelling, makes use of viewshed analysis based on digital terrain models (DTMs), digital surface models (DSMs), and vegetation distribution maps to simulate observations from a particular on-ground location (Aben, Signer, Heiskanen, Pellikka & Travis, 2021; Cimburova & Blumentrath, 2022; Labib et al., 2021). Some studies also incorporate 3D models of buildings as sight barriers, or to simulate the view from a particular floor-level in a building (Labib et al., 2021; Yu et al., 2016). The limitations of this approach result from the fact that DSMs and land-cover maps represent the vegetation simplified to its extent or canopy cover, while people see trees as 3D objects on the ground. Additionally, 3D building models are usually only available for large cities or city centres, and thus cannot be applied in regional or national studies.

The 3D quantification of vegetation across large regions and multiple sites has recently been addressed in the domain of visual ecology, which explores how visual information influences the spatial behaviour of animals. Using 3D point clouds from terrestrial laser scanning, Lecigne, Eitel and Rachlow (2020) successfully acquired very detailed information on the 3D structure of surrounding vegetation, and quantified the visible surroundings from single and multiple viewpoints. The data, however, must be collected separately at each individual location; the technology is therefore not suitable for large-scale studies.

The existing approaches for describing how people perceive the vegetation at a specific place are inadequate. The aim of this study is to contribute to filling this research gap. As part of the RESTORE project, we have developed a holistic concept and remote sensing, based on GIS and remote sensing, to describe green and natural places where people spend time to relieve stress caused by traffic noise.

The overall concept follows a three-level top–down approach. Each level relates to a different scale and amount of detail, as well as to the extent of the environment under consideration. At the highest level with the largest spatial extent, a bird's eye view provides information on land use, land cover, topography, viewshed, presence of natural and anthropogenic landscape features, accessibility, and noise levels, among other factors. The middle level focuses on a smaller spatial extent and provides more detailed insight into the 3D structure of the surrounding vegetation. The aim of the third, most detailed, level is to reconstruct the way a person sees their immediate environment. This level focuses on vegetation and considers obstructions of one landscape item by another. The present work deals exclusively with this third level of detail.

The aim of the study was to develop a reliable and computationally efficient method to quantify vegetation as seen from the human perspective which would be applicable over local, regional and country-wide scales, in particular in urban and suburban regions. To address the potentials and limitations noted above, we developed a solution based on ALS data. Namely, we used dense ALS point clouds to simulate a space observed from a particular on-ground location (Aben et al., 2018; Hamraz, Contreras, & Zhang, 2017). We completed all the data

processing and analysis in ArcGIS (v.10.8.1, ESRI) and the statistical software R (v.4.2.0; R Core Team, 2022), specifically the *lid*R package (v.4.0. 1; Roussel et al., 2020). *lid*R involves conventional ALS processing tools (e.g., ground classification, terrain interpolation, height normalization, construction of digital canopy models), and extraction of ALS metrics derived from the vertical elevation or intensity of the points. *lid*R also offers a highly flexible programming environment to implement innovative processing approaches (Roussel et al., 2020).

# 2 Data and Methods

## 2.1 Data

The main data sources used were ALS point clouds. Additionally, high-detail topographic data and DTM were utilized. The ALS data were acquired in the framework of a national campaign (SwissSurface3D) between 2017 and 2020, during the leaf-off season (early spring or late autumn), with an overall point density of ca. 15–20 points/m$^2$. The non-normalized ALS point clouds are available as LAS files (ASPRS LAS 1.2 Standard; ASPRS, 2008) and provide X, Y and Z point coordinates, as well as additional attributes such as point intensity, classification and return number.

The vector topographic data come from swissTLM3D, the most extensive and accurate large-scale 3D vector dataset of Switzerland (Swisstopo, 2022). The dataset describes the position, shape and many other attributes of almost 20 million natural and artificial landscape features across Switzerland. It comprises eight main categories (which are further divided into sub-categories): roads and tracks, public transport, buildings, areas with special use, land cover, hydrography, single point objects, and names (mountains, areas, towns etc.).

The corresponding DTM swissALTI3D provided by swisstopo is based on ALS data. It has an overall point density of 0.5 points per m$^2$ (Artuso et al., 2003), and a resolution of 2m, which was resampled to 1m.

## 2.2 Study area and sample locations

To develop the method, various sample locations across Switzerland were considered. These locations stemmed from an online survey focusing on destressing, where participants were asked to map the outdoor places in their everyday environment where they last went for restoration (restorative locations, RLs). The surroundings of the RLs were then described in terms of patterns and types of vegetation, including trees, shrubs and herbaceous vegetation, as well as open water areas and anthropogenic features, such as roads and paths.

## 2.3 Vegetation quantification from the human perspective

To reconstruct the human perspective of the surrounding space, it was assumed that a person sees their surroundings as a kind of virtual sphere with all the features (trees, buildings, ground surface etc.) and the sky projected onto it. The sphere was first divided into 180 latitudinal bands, each with a span of 1$^{o}$. Further, each band was divided into equal-area cells, from 360 cells at the observer's eye level to 1 cell at the zenith (Malkin, 2016). This avoided exaggeration of features (e.g., greenness) towards the zenith (Figure 1).

A circular 100m-wide buffer zone (referred to as a "plot" below) was created around each RL. The ALS sub-point clouds for each plot were extracted and stored in individual files. Subsequently, the human view in each location was reconstructed in four steps.

- The observer's horizontal (X, Y) location was determined as the centre of a plot; the vertical coordinate (Z) corresponded to the ground elevation plus the observer's height above the ground (2m).
- The plot point cloud was transformed from an orthogonal projection to an observer-centred projection, so that each point's coordinates were defined by the vertical angle (theta [θ], measured from -90$^{o}$ pointing vertically downwards to +90$^{o}$ at the zenith, with eye level at 0$^{o}$), the azimuth (fi [φ], measured clockwise starting from 0 in the north), and the distance to the point (r) (Figure 1).
- The surrounding virtual sphere was created and all the points in the cloud were projected on to it. Each cell of the sphere was assigned two values: (1) the distance from the observer to the nearest point (object); (2) the point's classification (vegetation, building and ground). The remaining cells were classified as sky or ground, when occurring above or below the horizon, respectively. A third attribute was the number of vegetation points visible from each cell.
- The derived attributes were used to calculate 80 sphere visibility metrics in three groups. They described: (1) the proportions of the sphere classified as ground, vegetation, building, water and sky, and the proportion of all above-ground cells; (2) the horizontal distribution of distance and the vertical distributions of the angles of the cells by classification, expressed by quantiles in 0.1 steps; and (3) the vegetation composition and density, expressed as the number, width and density of vegetation clumps. Initially, the counts of vegetation points in each horizontal direction were calculated based on the point cloud to assess vegetation presence or absence in each cell; the cells were attributed with values of 1 or 0, for presence or absence respectively. Then, sequences of at least 10 cells with repeating values of 1 were identified. These were considered vegetation clumps. Corrections were introduced for the northern azimuth, to merge vegetation detected at azimuths of 1$^{o}$ and 360$^{o}$. The width (the difference between the ending and starting azimuth), count of vegetation points, and density of vegetation points (the ratio of the count of vegetation points to the angular width of the clump) were calculated for each vegetation clump. Finally, the number of vegetation clumps

and the summarized (mean and standard deviation) characteristics of the individual clumps were calculated for each observer location.

For reference purposes, the sub-point clouds extracted earlier were normalized to obtain ground-related elevations; vegetation metrics traditionally used in research and practice (especially in the domains of forestry and ecology) were calculated, namely: maximum (zmax), mean (zmean), and standard deviation (zsd) of the height.

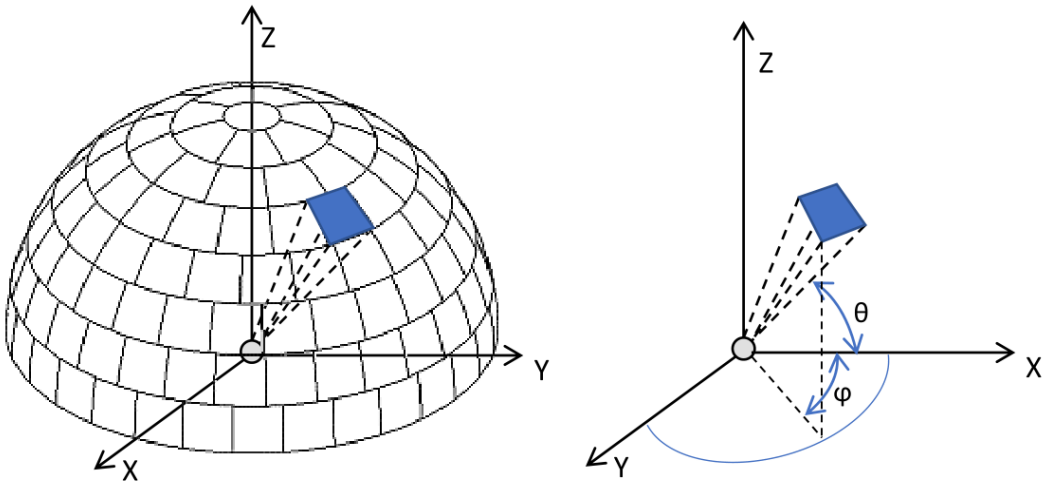


**Figure 1:** Illustration of the surrounding virtual sphere divided into equal-area cells. The observer is placed at the centre of the sphere, and the location of each cell is determined by two coordinates: vertical angle (θ) and azimuth (φ).

## 2.4 Performance assessment

The characteristics calculated for each site were assessed qualitatively for their plausibility and informational value by creating descriptive statistics and diagrams from the data of the spheres –for example, histograms of the horizontal and vertical depth distributions, or scatterplots of the distributions of the distances between the observer and non-obscured vegetation points. Orthophotos and topographic data were used to identify the land cover and objects present within the plot. Shaded relief maps and DTM provided information on the topographic context of each site. The spatial data, along with the simulations of RL-centred views of the 3D sub-point clouds, supported an investigation of the metrics obtained.

# 3 Results

The detailed performance of the method is demonstrated using the examples of two restorative locations: one in the forest (p20), and the other on arable land close to the forest edge (p53) (see Figure 2). These two landscape types and their combination were mentioned most

frequently (70%) as restorative sites by the survey participants. Other locations included riverbanks, lakeshores, open meadows and mountains.

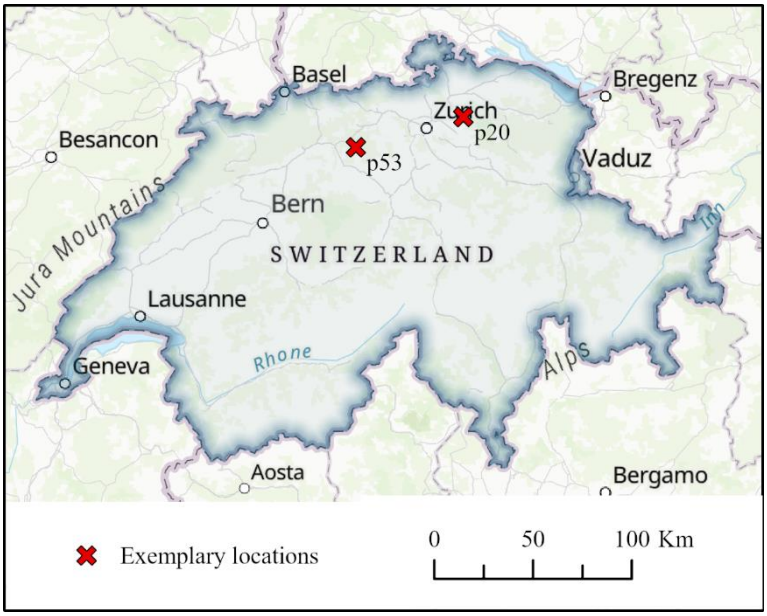


**Figure 2:** Location of the two exemplary restorative locations

## 3.1 Metric values and guide to interpretation

Of the metrics describing the elements of vegetation visible in the sphere, ten were particularly useful. They are listed and explained in Table 1.

**Table 1:** Metrics of particular importance for describing the vegetation from the human perspective.

| Variable | Explanation | Interpretation |
|---|---|---|
| PSVeg | Proportion of (all) sphere cells classified as vegetation | An indicator of how green the location looks from the observer's perspective; the higher the value, the more vegetation that can be seen; similar to the Greenness Visibility Index of Yang et al. (2009) |
| PSSky | Proportion of (all) sphere cells classified as sky | An indicator of the view's openness; the higher the value, the more sky that can be seen. |
| ThQVeg | Quantiles of the vertical viewing angle for all sphere cells classified as vegetation | The quantiles provide information on the vertical distribution of vegetation from the observer's perspective; high values of 0.9 or 1.0 quantiles indicate closed canopy cover over the observer (i.e., they are located under a tree). |

| | | |
|---|---|---|
| ThQSky | Quantiles of the vertical viewing angle for all sphere cells classified as sky | The quantiles provide information on the vertical distribution of the sky from the observer's perspective; low values of 0.0 or 0.1 quantiles indicate that the sky can be seen at lower elevations and may suggest that few of the surrounding features or little of the topography obscure the view. |
| PhiQVeg | Quantiles of the horizontal viewing angle for all sphere cells classified as vegetation | The quantiles provide information on the horizontal distribution of vegetation from the observer's perspective, e.g. clumping of vegetation. |
| PhiQSky | Quantiles of the horizontal viewing angle for all sphere cells classified as sky | The quantiles provide information on the horizontal distribution of the sky from the observer's perspective, i.e. the direction in which much of the (limited amount of) sky is visible. |
| DQVeg | Quantiles of distance for all sphere cells classified as vegetation | The quantiles provide information on the horizontal distribution of vegetation from the observer's perspective; the 0.0 quantile indicates how far the observer is from the closest vegetation object. |
| CLN | Number of vegetation clumps detected | A measure of visible vegetation groups. Even trees or shrubs growing at various distances from the observer may create a "green patch" for the observer. |
| mean_ CLW | Mean width of vegetation clumps | The width of a clump and the number of points within a clump provide information on the abundance or scarcity of vegetation within the clump. |
| mean_ CLNP | Mean number of points within the vegetation clumps | |

## 3.2 Example locations with different characteristics

The following paragraphs include descriptions of the two RLs and their surroundings, based on the measures derived from the method (Table 2) and the interpretation of the graphs (Figures 3 and 4).

**Table 2:** Selected ALS-based and sphere-based metrics for the exemplary RLs. Definitions of the variables (PSVeg etc.) are given in Table 1.

| | PSVeg | PSSky | CLN | mean_ CLW | | | | | | | |
|---|---|---|---|---|---|---|---|---|---|---|---|
| Forest | 56.3 | 31.6 | 1 | 360 | | | | | | | |
| Agricultural land | 5.4 | 32.7 | 2 | 64 | | | | | | | |
| Quantile | 0.0 | 0.1 | 0.2 | 0.3 | 0.4 | 0.5 | 0.6 | 0.7 | 0.8 | 0.9 | 1.0 |
| Vegetation distribution by distance (DQVeg) | | | | | | | | | | | |
| Forest | 2.7 | 18.4 | 22.8 | 25.6 | 28.6 | 31.8 | 35.7 | 40.9 | 47.4 | 58.4 | 99.9 |

| | | | | | | | | | | | |
|---|---|---|---|---|---|---|---|---|---|---|---|
| Agricultural land | 47.6 | 51.9 | 54.7 | 58.2 | 68.1 | 73.3 | 75.5 | 78.8 | 81.7 | 86.9 | 100.0 |
| Vegetation distribution by azimuthal angle | | | | | | | | | | | |
| Forest | 0 | 27 | 66 | 113 | 157 | 195 | 231 | 260 | 292 | 330 | 360 |
| Agricultural land | 0 | 35 | 70 | 105 | 143 | 179 | 216 | 252 | 288 | 324 | 360 |
| Vegetation distribution by vertical angle | | | | | | | | | | | |
| Forest | 1 | 30 | 42 | 51 | 59 | 66 | 73 | 80 | 87 | 98 | 140 |
| Agricultural land | 66 | 73 | 76 | 78 | 80 | 82 | 84 | 85 | 87 | 89 | 97 |
| Sky distribution by azimuthal angle | | | | | | | | | | | |
| Forest | 0.0 | 53.8 | 92.0 | 124.0 | 152.7 | 180.7 | 209.1 | 239.2 | 270.8 | 306.3 | 360.0 |
| Agricultural land | 0.0 | 35.7 | 76.2 | 117.8 | 157.3 | 192.8 | 227.2 | 260.5 | 293.7 | 326.9 | 360.0 |
| Sky distribution by vertical angle | | | | | | | | | | | |
| Forest | 91 | 110 | 116 | 122 | 128 | 133 | 138 | 144 | 151 | 160 | 180 |
| Agricultural land | 99 | 112 | 117 | 122 | 127 | 132 | 137 | 143 | 150 | 159 | 180 |

## 3.3 Forest (p20)

The first RL is located in closed-canopy forest. According to the sphere-based results (Table 2), 56.3% of the cells were classified as vegetation, 31.6% as sky, and 8.1% as ground. Half of the visible vegetation occurred between 2.7m and 31.8m (DQ_0.0Veg and DQ_0.5Veg) from the observer. In the vertical dimension, half of the visible vegetation occurred below $24^{o}$ and values reached $89^{o}$, which means that the ground was covered with vegetation and the canopy was closed above the observer's head. The vegetation clump identified as having a width of $360^{o}$ signals that the location was completely surrounded by vegetation.

The histogram in Figure 3D shows that the visible ground was located closer to the observer than the visible vegetation, mostly no more than about 30m away. The visible vegetation was distributed throughout the 100m zone, but distances of about 25m were the most frequent.

As shown in Figure 3E, the ground was visible below eye level in the north (azimuthal angle around $0^{o}$), and at eye level ($0^{o}$) in the south (azimuthal angle around $180^{o}$). This means that the terrain descended towards the north and remained on a similar elevation to the observer, which can also be interpreted from Figure 3C. Consequently, the vegetation was visible above ground level, at lower vertical angles to the north and higher vertical angles to the south. This can also be seen in Figure 3F, which presents all vegetation points in the cloud within the plot, coloured by vertical angle, in an overhead view. Most of the points in the north are assigned negative vertical angles, while more positive values are found in the south. At vertical angles close to $0^{o}$, some vegetation located far away from the observer can be seen, which is not the case at large vertical angles (Figure 3E). Figure 3G shows that the vegetation is densest in the north and sparser in the south.

## 3.4 Agricultural land with forest patches (p53)

The second RL is dominated by agricultural land, with small patches of forest and shrubs encroaching from the north and west, on mostly flat terrain, the eastern part of which slopes gently down towards the east (Figures 4A, 4B, 4C). In the sphere-based results (Table 2), 5.4% of the cells were classified as vegetation, 32.7% as sky, and 13.3% as ground. Visible vegetation did not completely surround the RL but appeared in two clumps of average width equal to 64$^{o}$. The nearest visible vegetation was 47.6m from the observer (DQ_0.0Veg), and the closer distances were dominated by ground (Figure 4D). As the histogram of the distance-to-visible-vegetation shows, the two vegetation clumps detected were located around 50–60m and 70–100m from the observer (Figure 4D). A single vegetation feature (too small to be detected as a clump) occurred at the azimuth of approximately 135$^{o}$, on the gentle slope below the observer's eye level (Figure 4E).

In the vertical dimension, half of the visible vegetation occurred below 8$^{o}$, and values reached 24$^{o}$, which means there was a large proportion of sky visible around and above the observer. As shown in Figure 4E, almost all ground was visible at and below the observer's eye level; only towards the east did the ground gently slope away (azimuthal angle around 90$^{o}$), which can also be interpreted from Figure 4C. Accordingly, the vegetation was visible above the ground level (and the observer's eye level). This can also be seen in Figure 4F, where most of the vegetation points are assigned positive values, though noticeably lower ones than in the case of the forest RL (p20). Figure 4G shows similar numbers of vegetation points within the two clumps detected and confirms the small size of the single vegetation feature in the south-east.

**Explanation for Figures 3 and 4.**
Row 1: Exemplary restorative locations (RLs) shown on: an orthophoto map (A), a vegetation height model (B), and a coloured and shaded relief map (C). Row 2: Sphere-cell-based statistics: distribution of distances for all sphere cells classified as ground or vegetation (D); horizontal and vertical distributions of sphere cells classified as ground or vegetation, coloured by distance from the observer (E). Row 3: overhead view of sphere cells classified as vegetation, coloured by vertical angle theta (F); distribution of all vegetation points in the cloud by azimuthal angle (G).

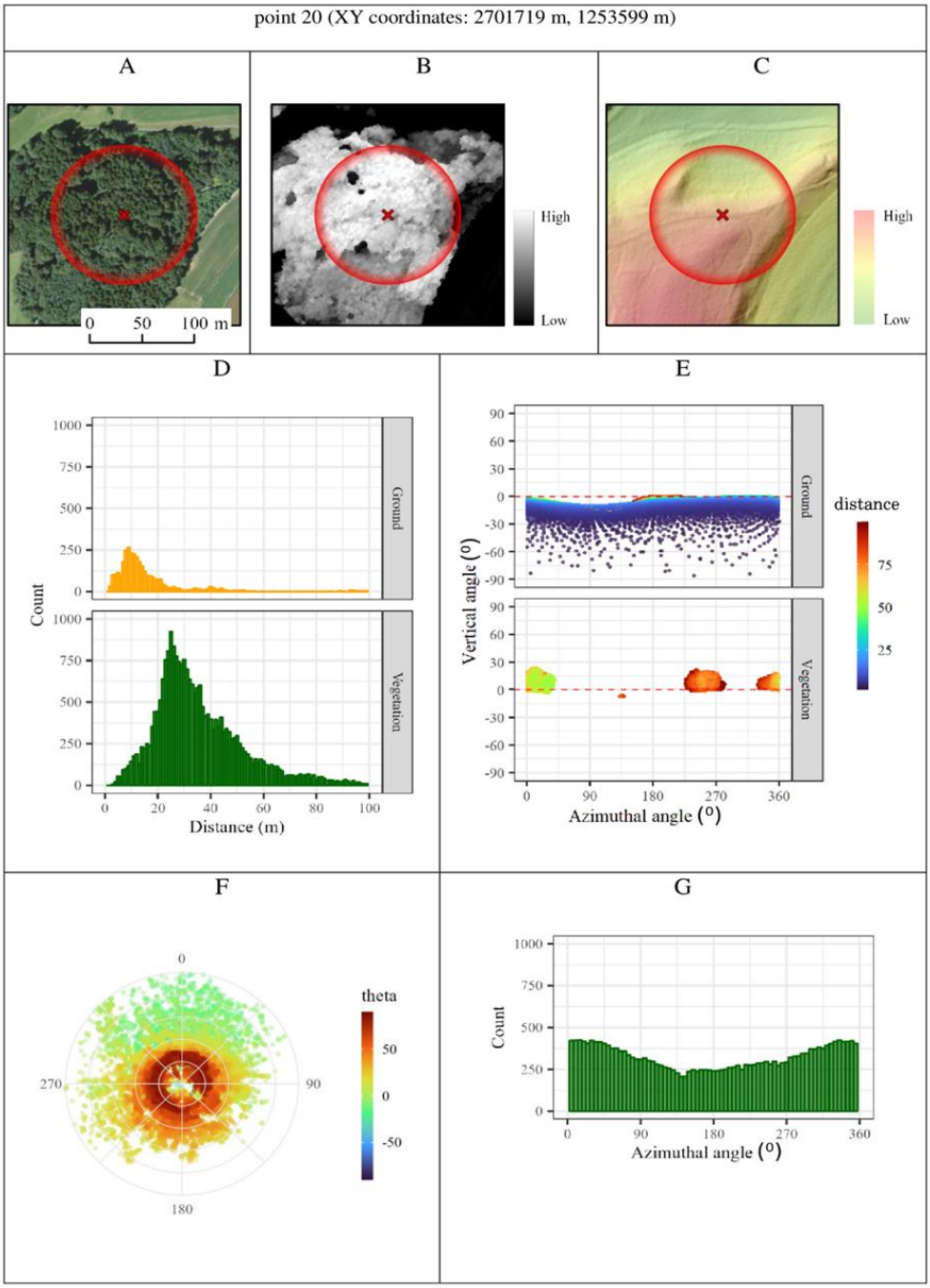


**Figure 3:** Forest (p20)

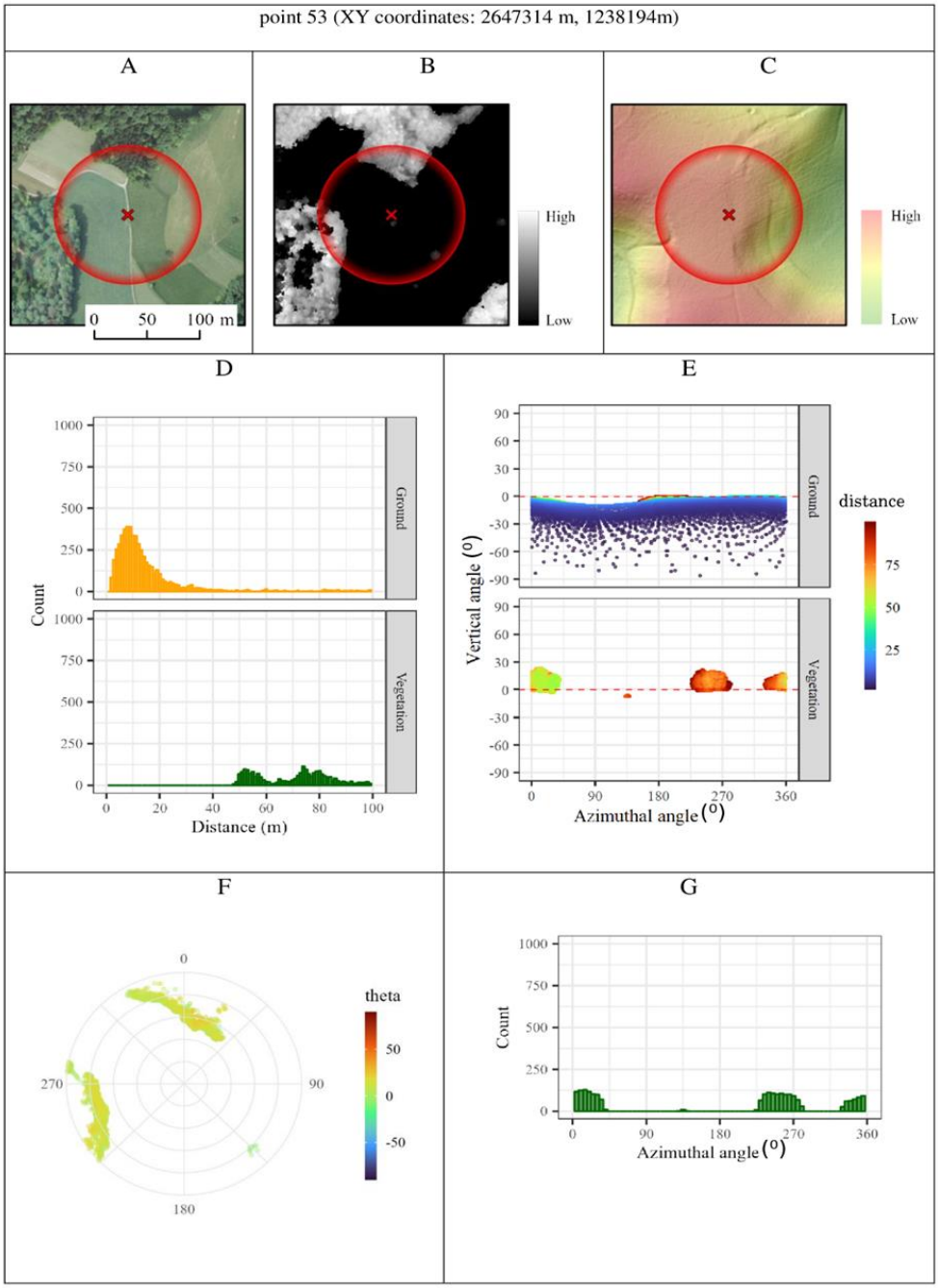


**Figure 4**: Agricultural land with forest patches (p53)

## 4 Discussion and conclusion

Using 3D remote sensing data and additional spatial data, we developed a method for quantifying visible vegetation located nearby from a human perspective. The method is highly automated and can be applied in a dense grid on a small scale, as well as over large areas. Based on ALS point clouds, we simulated a space viewed from a specific location and characterized the surrounding nearby vegetation in detail. We applied this new method to a number of specific green and natural places that are important for people to recover from noise-related stress in everyday life.

Our method combines highly automated and efficient algorithms which enable detailed analysis from many different observation points. We developed a guide for interpreting the variables calculated, with illustrative examples, to minimize the expert knowledge and manual operations required. The great strength of this method is its transferability to other sites. Wherever ALS point clouds with a point density similar to that in our study or higher are available, vegetation structures can be quantified from a human perspective. Unlike well-known photo-based methods (Kumakoshi et al., 2020; Li et al., 2015; Yang et al., 2009), our approach is not limited to street views and can be applied over a wide area. The virtual sphere mimics the photo-based approach while preserving the 3D vegetation structure (Chen et al., 2015). The visual importance of the terrain and features (Nutsford et al., 2015) is captured by calculating the vertical angle and both the distance to, and the density of, vegetation. Finally, the over-weighting of features towards the zenith is avoided.

Another great advantage of the method is its versatility, as it can be applied in both natural and urban environments. It considers occlusions by terrain and buildings and thus identifies the vegetation that is actually visible. In small-scale urban areas, it additionally provides information on the horizontal and vertical distributions of nearby buildings and visible sky, which have a significant influence on the restorative effect (Kent & Schiavon, 2020). Furthermore, the size of the buffer around the sites being studied (which depends on the definition of "what is close") can be adapted to the needs of specific situations.

This method can provide valuable information in urban areas where green spaces have a special importance for local people and for spatial planning. An illustrative application of the method is the RESTORE project, where we will compare the visible share of green quantified in this way with survey results on the perceived restorative quality of specific landscapes. This will allow the identification of those landscape characteristics of green spaces that have high restorative quality. The method can be applied at different spatial scales, provides methodological support for spatial planning, and is particularly suitable for large-scale socio-ecological studies on the influence of the "view into the green" on health and wellbeing.

## References


Aben, J., Pellikka, P., & Travis, J. M. J. (2018). A call for viewshed ecology: advancing our understanding of the ecology of information through viewshed analysis. *Methods in Ecology and Evolution*, *9*(3), 624–633. https://doi.org/10.1111/2041-210X.12902

Aben, J., Signer, J., Heiskanen, J., Pellikka, P., & Travis, J. M. J. (2021). What you see is where you go: visibility influences movement decisions of a forest bird navigating a three-dimensional-structured matrix. *Biology Letters*, *17*(1). https://doi.org/10.1098/rsbl.2020.0478

Artuso, R., Bovet, S., & Streilein, A. (2003). Practical methods for the verification of countrywide terrain and surface models. *International Archives for Photogrammetry, …*, 0–5. http://www.isprs.org/proceedings/XXXIV/3-W13/papers/Artuso_ALSDD2003.pdf

ASPRS. (2008). *LAS Specification, version 1.2* pp. 1–13. American Society of Photogrammetry and Remote Sensing. Retrieved from https://www.asprs.org/divisions-committees/lidar-division/laser-las-file-format-exchange-activities

Bell, S. (2010). Forest recreation and nature tourism. *Urban Forestry and Urban Greening*, *9*(2), 69–70. https://doi.org/10.1016/j.ufug.2010.03.001

Bezold, C. P., Banay, R. F., Coull, B. A., Hart, J. E., James, P., Kubzansky, L. D., … Laden, F. (2018). The relationship between surrounding greenness in childhood and adolescence and depressive symptoms in adolescence and early adulthood. *Annals of Epidemiology*, *28*(4), 213–219. https://doi.org/10.1016/j.annepidem.2018.01.009

Chen, Z., Xu, B., & Gao, B. (2015). Assessing visual green effects of individual urban trees using airborne Lidar data. *Science of the Total Environment*, *536*, 232–244. https://doi.org/10.1016/j.scitotenv.2015.06.142

Cimburova, Z., & Blumentrath, S. (2022). Viewshed-based modelling of visual exposure to urban greenery – an efficient GIS tool for practical planning applications. *Landscape and Urban Planning*, *222*(February), 104395. https://doi.org/10.1016/j.landurbplan.2022.104395

Davison, S., Donoghue, D. N. M., & Galiatsatos, N. (2020). The effect of leaf-on and leaf-off forest canopy conditions on LiDAR derived estimations of forest structural diversity. *International Journal of Applied Earth Observation and Geoinformation*, *92*(June), 102160. https://doi.org/10.1016/j.jag.2020.102160

Degerickx, J., Hermy, M., & Somers, B. (2020). Mapping functional urban green types using high resolution remote sensing data. *Sustainability (Switzerland)*, *12*(5), 1–35. https://doi.org/10.3390/su12052144

Goodbody, T. R. H., Tompalski, P., Coops, N. C., Hopkinson, C., Treitz, P., & van Ewijk, K. (2020). Forest inventory and diversity attribute modelling using structural and intensity metrics from multi-spectral airborne laser scanning data. *Remote Sensing*, *12*(13). https://doi.org/10.3390/rs12132109

Hamraz, H., Contreras, M. A., & Zhang, J. (2017). Forest understory trees can be segmented accurately within sufficiently dense airborne laser scanning point clouds. *Scientific Reports*, *7*(1), 1–9. https://doi.org/10.1038/s41598-017-07200-0

James, P., Banay, R. F., Hart, J. E., & Laden, F. (2015). A review of the health benefits of greenness. *Current Epidemiology Reports*, *2*(2), 131–142. https://doi.org/10.1007/s40471-015-0043-7

Jiang, B., Deal, B., Pan, H. Z., Larsen, L., Hsieh, C. H., Chang, C. Y., & Sullivan, W. C. (2017). Remotely-sensed imagery vs. eye-level photography: evaluating associations among measurements of tree cover density. *Landscape and Urban Planning*, *157*, 270–281. https://doi.org/10.1016/j.landurbplan.2016.07.010

Kent, M., & Schiavon, S. (2020). Evaluation of the effect of landscape distance seen in window views on visual satisfaction. *Building and Environment*, *183*(August), 107160. https://doi.org/10.1016/j.buildenv.2020.107160

Keränen, J., Maltamo, M., & Packalen, P. (2016). Effect of flying altitude, scanning angle and scanning mode on the accuracy of ALS based forest inventory. *International Journal of Applied Earth Observation and Geoinformation*, *52*, 349–360. https://doi.org/10.1016/j.jag.2016.07.005

Kumakoshi, Y., Chan, S. Y., Koizumi, H., Li, X., & Yoshimura, Y. (2020). Standardized green view index and quantification of different metrics of urban green vegetation. *Sustainability (Switzerland)*, *12*(18), 1–16. https://doi.org/10.3390/SU12187434

Labib, S. M., Huck, J. J., & Lindley, S. (2021). Modelling and mapping eye-level greenness visibility exposure using multi-source data at high spatial resolutions. *Science of the Total Environment*, *755*, 143050. https://doi.org/10.1016/j.scitotenv.2020.143050

Lecigne, B., Eitel, J. U. H., & Rachlow, J. L. (2020). viewshed3d: an R package for quantifying 3D visibility using terrestrial lidar data. *Methods in Ecology and Evolution*, *11*(6), 733–738. https://doi.org/10.1111/2041-210X.13385

Li, X., Zhang, C., Li, W., Ricard, R., Meng, Q., & Zhang, W. (2015). Assessing street-level urban greenery using Google Street View and a modified green view index. *Urban Forestry and Urban Greening*, *14*(3), 675–685. https://doi.org/10.1016/j.ufug.2015.06.006

Malkin, Z. (2016). *A new method to subdivide a spherical surface into equal-area cells*. Retrieved from http://arxiv.org/abs/1612.03467

Nutsford, D., Reitsma, F., Pearson, A. L., & Kingham, S. (2015). Personalising the viewshed: Visibility analysis from the human perspective. *Applied Geography*, *62*, 1–7. https://doi.org/10.1016/j.apgeog.2015.04.004

Palliwoda, J., & Priess, J. A. (2021). What do people value in urban green? Linking characteristics of urban green spaces to users' perceptions of nature benefits, disturbances, and disservices. *Ecology and Society*, *26*(1). https://doi.org/10.5751/ES-12204-260128

Pirotti, F. (2011). Analysis of full-waveform LiDAR data for forestry applications: a review of investigations and methods. *IForest*, *4*(JUNE), 100–106. https://doi.org/10.3832/ifor0562-004

R Core Team. (2022). R: A language and environment for statistical computing. Retrieved October 25, 2022, from https://www.r-project.org/

Roussel, J. R., Auty, D., Coops, N. C., Tompalski, P., Goodbody, T. R. H., Meador, A. S., … Achim, A. (2020). lidR: an R package for analysis of Airborne Laser Scanning (ALS) data. *Remote Sensing of Environment*, *251*(August), 112061. https://doi.org/10.1016/j.rse.2020.112061

Shahtahmassebi, A. R., Li, C., Fan, Y., Wu, Y., lin, Y., Gan, M., … Blackburn, G. A. (2021). Remote sensing of urban green spaces: a review. *Urban Forestry and Urban Greening*, *57*(December 2020), 126946. https://doi.org/10.1016/j.ufug.2020.126946

Swisstopo. (2022). Topographic Landscape Model TLM. Retrieved from https://www.swisstopo.admin.ch/en/knowledge-facts/topographic-landscape-model.html

Wood, L., Hooper, P., Foster, S., & Bull, F. (2017). Public green spaces and positive mental health – investigating the relationship between access, quantity and types of parks and mental wellbeing. *Health and Place*, *48*(September), 63–71. https://doi.org/10.1016/j.healthplace.2017.09.002

World Bank. (2022). Retrieved October 13, 2022, from Urban population (% of total population) website: https://data.worldbank.org/indicator/SP.URB.TOTL.IN.ZS

Yang, J., Zhao, L., Mcbride, J., & Gong, P. (2009). Can you see green? Assessing the visibility of urban forests in cities. *Landscape and Urban Planning*, *91*(2), 97–104. https://doi.org/10.1016/j.landurbplan.2008.12.004

Yu, S., Yu, B., Song, W., Wu, B., Zhou, J., Huang, Y., … Mao, W. (2016). View-based greenery: A three-dimensional assessment of city buildings' green visibility using Floor Green View Index. *Landscape and Urban Planning*, *152*, 13–26. https://doi.org/10.1016/j.landurbplan.2016.04.004

Zeng, Y., Hao, D., Huete, A., Dechant, B., Berry, J., Chen, J. M., … Chen, M. (2022). Optical vegetation indices for monitoring terrestrial ecosystems globally. *Nature Reviews Earth and Environment*, *3*(7), 477–493. https://doi.org/10.1038/s43017-022-00298-5